electronics

MDPI

Article

Performance Analysis and Game-Based Bandwidth Allocation for UL/DL Decoupled C-V2X

Luofang Jiao [1,2,*], Pin Li [1,2], Yuhao Yang [1,2], Linghao Xia [1,2], Qiang Cheng [1,2], Xingwei Ye [1,2], Jingbei Yang [1,2] and Xianzhe Xu [1,2]

[1] Nanjing Research Institute of Electronics Technology, Nanjing 210023, China; dtpinl@163.com (P.L.); yyhao@mail.ustc.edu.cn (Y.Y.); xlh2006@163.com (L.X.); cqchengqiang@sina.com (Q.C.); ye_xingwei@yeah.net (X.Y.); yjb014@sina.com (J.Y.); august.xxz@alumni.sjtu.edu.cn (X.X.)
[2] National Key Laboratory of Radar Detection and Sensing, Nanjing 210023, China
* Correspondence: luofang_jiao@smail.nju.edu.cn; Tel.: +86-13951653075

Abstract

Uplink/downlink (UL/DL) decoupled access has emerged as a promising paradigm for heterogeneous cellular vehicle-to-everything (C-V2X) networks in beyond 5G (B5G) and 6G systems. In multi-operator scenarios, wireless service provider (WSP) selection becomes critical for vehicles to ensure communication quality while minimizing costs. This paper investigates the performance analysis and WSP selection problem in UL/DL decoupled access C-V2X networks. We derive tractable expressions for spectral efficiency of both UL and DL using stochastic geometry, considering three decoupled access cases where UL and DL independently associate with macro base stations (MBSs) or small base stations (SBSs). We formulate a hierarchical game framework combining evolutionary game for vehicle WSP selection and non-cooperative game for WSP bandwidth allocation. An evolutionary game algorithm is proposed to reach the equilibrium, and the uniqueness of Nash equilibrium in bandwidth allocation is proved. Extensive simulations validate the analytical results and demonstrate the convergence and stability of the proposed game framework.

Keywords: C-V2X; UL/DL decoupled access; wireless service provider; spectral efficiency; evolutionary game; stochastic geometry

1. Introduction

With the rapid advancement of the beyond fifth generation (B5G) and sixth generation (6G) mobile communication technology, cellular vehicle-to-everything (C-V2X) has emerged as a key enabler for intelligent transportation systems (ITSs) and integrated sensing and communication (ISAC) [1], supporting diverse vehicular applications such as autonomous driving, cooperative perception, and real-time traffic management [2–4]. The number of connected vehicles is expected to grow exponentially, leading to unprecedented challenges in network capacity, coverage, and quality of service (QoS) provisioning. To address these challenges, C-V2X has evolved towards heterogeneous cellular networks (HCNs), which integrate macro base stations (MBSs) and small base stations (SBSs) to provide ubiquitous coverage and enhanced capacity [5–7].

In traditional cellular networks, uplink (UL) and downlink (DL) transmissions are coupled, meaning that user equipment (UE) must associate with the same base station (BS) for both UL and DL communications [8]. However, this coupled access paradigm faces significant limitations in heterogeneous C-V2X networks [9]. The asymmetry between UL and DL traffic patterns becomes more pronounced, with DL typically requiring

Check for updates

Academic Editors: Annamaria Sarbu, Angela Digulescu, Cornel Ioana, Emanuel Puschita and Cristina Despina-Stoian

Received: 29 March 2026
Revised: 16 April 2026
Accepted: 20 April 2026
Published: 24 April 2026

Copyright: © 2026 by the authors. Licensee MDPI, Basel, Switzerland. This article is an open access article distributed under the terms and conditions of the Creative Commons Attribution (CC BY) license.

higher data rates for content delivery while UL demands lower latency for safety-critical messages [9]. Moreover, the transmit power imbalance between MBSs and SBSs creates coverage asymmetry, where vehicles at cell edges experience poor UL performance due to limited transmit power [10]. The high mobility of vehicles and dynamic network topology further exacerbate the interference and handover issues in dense urban environments [11].

UL/DL decoupled access technology has been proposed as a promising solution to address these limitations [10,12,13]. In UL/DL decoupled access, UL and DL transmissions are separated and can be allocated to different BSs, allowing vehicles to independently select the optimal BS for each direction based on signal quality, interference conditions, and QoS requirements [14,15]. This flexibility is particularly beneficial in heterogeneous C-V2X networks where BSs with different transmit powers, coverage areas, and backhaul capacities coexist. Vehicles can associate with nearby SBSs for UL transmission to reduce path loss and transmit power while maintaining DL connection with MBSs that provide higher data rates.

Despite the potential benefits of UL/DL decoupled access, several critical challenges remain in practical deployments. First, the performance analysis of UL/DL decoupled access in C-V2X networks is complex due to the unique characteristics of vehicular mobility and road topology. Stochastic geometry has emerged as a powerful tool for tractable performance analysis by modeling BS locations as spatial point processes [5,16]. Second, in multi-operator scenarios, multiple wireless service providers (WSPs) may coexist and compete for vehicle users by offering different service qualities and pricing strategies. How vehicles select appropriate WSPs while ensuring their communication requirements becomes a critical problem. Third, WSPs need to optimize their bandwidth allocation strategies to maximize revenue while considering the competition from other WSPs and the dynamic behavior of vehicles. Game theory provides a natural framework to model such strategic interactions [17,18]. These challenges motivate our work to develop a comprehensive framework that jointly addresses performance analysis, WSP selection, and bandwidth allocation in UL/DL decoupled access C-V2X networks.

The main contributions of this paper are as follows:

- We derive tractable spectral efficiency expressions for UL/DL decoupled access C-V2X using stochastic geometry and obtain the corresponding association probabilities and conditional distance distributions for the three decoupled access cases.
- We establish a hierarchical game framework for the multi-WSP UL/DL decoupled access problem, where the lower-level evolutionary game models vehicle WSP selection and the upper-level non-cooperative game determines the bandwidth allocation of each WSP. We further prove the uniqueness of the Nash equilibrium.
- We develop the corresponding iterative algorithms and verify through simulations the convergence, stability, and performance of the proposed framework under different network settings, including the effects of network density on payoff evolution, user distribution, and bandwidth allocation.

The remainder of this paper is organized as follows. We briefly introduce the existing research works related to UL/DL decoupled access and game theory in Section 2. Section 3 presents the channel and interference model for C-V2X. Then the performance for UL/DL decoupled access, the game scheme, and an evolutionary game algorithm are given to solve the issues in Section 4. The numerical and simulation results are presented and discussed in Section 5 and this paper is concluded in Section 6.

2. Related Work

2.1. Performance Analysis of Heterogeneous Networks

Stochastic geometry has emerged as a powerful mathematical tool for modeling and analyzing wireless networks. Andrews et al. [5] pioneered the use of Poisson point processes (PPPs) to model BS locations and derived tractable expressions for coverage probability and achievable rate in cellular networks. This seminal work established the foundation for analytical performance evaluation without requiring extensive simulations. Building on this framework, Dhillon et al. [19] extended the analysis to K-tier heterogeneous networks, where different tiers of BSs (macro, pico, femto) coexist with different transmit powers and densities. Jo et al. [20] further investigated flexible cell association strategies in heterogeneous networks and provided comprehensive SINR analysis. For vehicular networks specifically, Chetlur et al. [16] modeled vehicular networks as Cox processes driven by Poisson line processes to capture the road topology, and derived coverage probability expressions for vehicle-to-infrastructure communications. Lu et al. [21] provided a comprehensive tutorial on stochastic geometry analysis for spatial–temporal performance in wireless networks. However, these works primarily focus on traditional coupled access scenarios where UL and DL are associated with the same BS.

2.2. UL/DL Decoupled Access

UL/DL decoupled access has been proposed as a promising solution to address the coverage imbalance problem in heterogeneous networks. Elshaer et al. [10] first demonstrated that decoupling UL and DL cell associations can provide substantial performance gains, especially for cell-edge users who suffer from limited UL transmit power. They showed that allowing UEs to associate with different BSs for UL and DL based on respective signal strengths can significantly improve both coverage and throughput. Sattar et al. [22] derived analytical expressions for spectral efficiency in two-tier networks with decoupled access using stochastic geometry and quantified the performance gains compared to traditional coupled access. In the context of C-V2X networks, Wu et al. [11] analyzed uplink transmission performance in user-centric ultra-dense vehicle-to-infrastructure networks, where vehicles can flexibly select serving BSs. Jiao et al. [9] investigated spectral efficiency of UL/DL decoupled access in C-V2X networks and analyzed the impact of various system parameters. More recently, Jiao et al. [15] proposed joint optimization algorithms for flexible decoupled access in heterogeneous C-V2X communications. Despite these advances, existing works focus on single-operator scenarios and do not consider the multi-WSP competition and selection problem.

2.3. Game Theory for Network Selection and Resource Allocation

Game theory provides a powerful framework for modeling strategic interactions in multi-operator wireless networks. In the context of network selection, Xu et al. [17] proposed a hierarchical game framework that combines evolutionary game at the lower level for user network selection and non-cooperative game at the upper level for WSP bandwidth allocation in multi-tier heterogeneous cellular networks. Their work demonstrated that the hierarchical game can effectively model the two-level interactions and achieve stable equilibrium. Kazmi et al. [18] developed a hierarchical game-theoretic approach for network selection in heterogeneous wireless networks, considering both user preferences and network conditions. For resource allocation, Wu et al. [23] proposed a revenue sharing-based resource allocation scheme for dynamic spectrum access networks, but their centralized approach requires extensive information exchange between users and WSPs, leading to high communication overhead and operational costs. Niyato et al. [24] investigated competitive pricing for spectrum sharing in cognitive radio networks using

dynamic game theory and analyzed the inefficiency of Nash equilibrium. In vehicular networks, Qian et al. [3] proposed a dynamic Stackelberg pricing game for multi-mode spectrum sharing in 5G-VANET, where infrastructure operators act as leaders and vehicular users act as followers. Liang et al. [25] applied multi-agent reinforcement learning for spectrum sharing in vehicular networks. However, these existing works primarily consider traditional coupled access scenarios and do not address the unique characteristics and challenges of UL/DL decoupled access in multi-operator C-V2X networks, where vehicles need to make independent association decisions for UL and DL transmissions.

Motivated by the above issues, this paper studies UL/DL decoupled access C-V2X in a multi-WSP scenario. We analyze the spectral efficiency of three decoupled access cases, formulate the joint problem of vehicle WSP selection and WSP bandwidth allocation as a hierarchical game, and evaluate its convergence and performance under different network configurations.

3. System Model

3.1. Modeling of C-V2X Network

To analyze the performance tractably, a C-V2X network is modeled in a 2-D Euclidean plane. The network consists of MBSs ϖ_m with density λ_m following the distribution of a 2-D Poisson point process (PPP), SBSs ϖ_s with density λ_s deployed along the roads following a 1-D PPP, and vehicles ϖ_v with density λ_v is deployed in terms of an independent homogeneous 1-D PPP on a road. The roads are modeled as a Poisson line process (PLP) ϖ_l with intensity λ_l. We assume a standard path-loss model $x^{-\alpha}, (\alpha > 2)$ and α is the path-loss exponent parameter, x is the distance between the BS and vehicle. The channel gains are denoted as h_m, h_s for the channel between the vehicle with an MBS, and the vehicle with an SBS, respectively. Here h_m and h_s represent the deterministic antenna and propagation gains, which are fixed and distinct from the random fading components [16]. The fadings are modeled as the Rayleigh fading g_m, g_s and $g \sim exp(\mu)$. Since the shadowing effects ε make the receiving power not exponentially distributed, we use random displacement to solve this issue as in [26]. Thus the transformed MBSs, SBSs, and vehicles are denoted as $\varpi_m^t, \varpi_s^t, \varpi_v^t$ with $\lambda_m^t = E\left[\varepsilon^{-\frac{2}{\alpha}}\right]\lambda_m, \lambda_s^t = E\left[\varepsilon^{-\frac{1}{\alpha}}\right]\lambda_s, \lambda_v^t = E\left[\varepsilon^{-\frac{1}{\alpha}}\right]\lambda_v$, respectively. The $E\left[\varepsilon^{-\frac{2}{\alpha}}\right]\lambda_m$ for a 2-D PPP can be calculated as

$$E\left[\varepsilon^{-\frac{2}{\alpha}}\right]\lambda = \exp\left(\frac{\omega \ln 10}{10\alpha} + \frac{1}{2}\left(\frac{\sigma \ln 10}{10\alpha}\right)^2\right)\lambda. \tag{1}$$

The $E\left[\varepsilon^{-\frac{1}{\alpha}}\right]\lambda_m$ for a 1-D PPP can be calculated following similar steps. Thus the received signal powers (RSPs) of UL and DL are

$$\begin{cases} RSP_d = P_d g_d h_d x^{-\alpha_d}, d = \{m, s\} \\ RSP_u = P_v g_v h_u x^{-\alpha_v}, u = \{m, s\} \end{cases}, \tag{2}$$

where P_m, P_s, and P_v are the transmit powers of the MBS, SBS, and vehicle, respectively.

3.2. Interference

We choose a vehicle at origin $(0, 0)$ and call it the typical vehicle x_o; the corresponding road is called a typical road. The signal-to-interference-plus-noise ratio (SINR) of UL at x_o is

$$SINR_u = \frac{RSP_u}{I_u + \sigma_u^2}, u = \{m, s\}, \tag{3}$$

where the interference I_u is $I_u = I_u^t + I_u^o$, I_u^t is the interference from the vehicles on the typical road $\varpi_{v,o}^t \backslash x_o$, and I_u^o is the interference from the vehicles on the other roads $\varpi_{v,l}^t$ [27].

$$I_u^t = \sum_{i \in \left\{\varpi_{v,o}^t \backslash x_o\right\}} P_v g_u h_u x_i^{-\alpha_u}, u = \{m, s\}, \tag{4}$$

$$I_u^o = \sum_{i \in \left\{\varpi_{v,l}^t\right\}} P_v g_u h_u^o x_i^{-\alpha_u}, u = \{m, s\}. \tag{5}$$

Similarly, the SINR at the typical vehicle in DL is

$$SINR_d = \frac{RSP_d}{I_d + \sigma_d^2}, d = \{m, s\}, \tag{6}$$

where, when being connected to an MBS, the interference I_d is

$$I_d = \sum_{i \in \left\{\varpi_m^t \backslash x_o\right\}} P_m g_m h_m x_i^{-\alpha_m}, \tag{7}$$

and when associating with an SBS, $I_u = I_d^t + I_d^o$,

$$I_d^t = \sum_{i \in \left\{\varpi_{s,o}^t \backslash x_o\right\}} P_s g_s h_s x_i^{-\alpha_s}, \tag{8}$$

$$I_d^o = \sum_{i \in \varpi_{s,l}^t} P_s g_s h_s^o x_i^{-\alpha_s}. \tag{9}$$

4. Performance Analysis and Game Scheme

4.1. Ul/Dl Decoupled Access C-V2X

In UL/DL decoupled access C-V2X networks, vehicles can choose one BS for DL and another for UL, contrasting with coupled access that uses a single BS for both [15]. For the coupled access baseline, both UL and DL are associated with the same BS, and the serving BS is selected according to the strongest downlink received signal power criterion. In heterogeneous C-V2X, we deploy two types of BSs, i.e., the MBS and SBS as shown in Figure 1, along the roads. Thus there are three decoupled access modes as follows:

- Case 1 : DL = MBS 1, UL = MBS 2;
- Case 2 : DL = MBS 1, UL = SBS 1;
- Case 3 : DL = SBS 1, UL = SBS 2.

For Cases 1 and 3, UL and DL remain on the same tier but associate with different BSs. The decoupled gain in these cases arises because DL and UL follow different association criteria; therefore, the nearest BS for DL may differ from that for UL, even within the same tier.

4.2. Spectral Efficiency

Spectral efficiency refers to the rate at which information can be transmitted over a unit bandwidth [28].

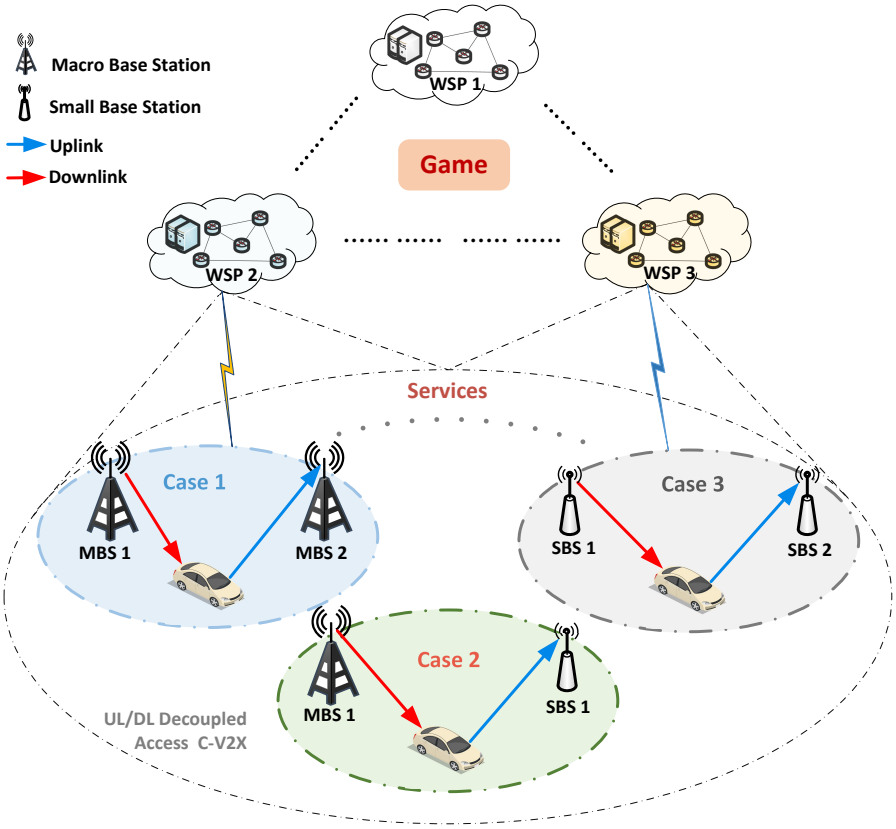


Figure 1. A game-based multiple WSPs selection scheme for UL/DL decoupled access C-V2X.

Lemma 1. *The spectral efficiency of UL for Case 1 is formulated as*

$$\tau_u^1 = \int_0^\infty f_{m,1}(x) E[\ln(1 + SINR_u)] dx, \tag{10}$$

where $E[\ln(1 + SINR_d)]$ *is*

$$E[\ln(1 + SINR_u)] = \int_0^\infty e^{-\frac{\left(e^t - 1\right) x^{\alpha_m} \sigma_u^2}{P_v h_m}} \zeta_{I_u}(j) dt, \tag{11}$$

where $j = \frac{\left(e^t - 1\right) x^{\alpha_m}}{P_v h_m}$, $\zeta_{I_u}(j) = \zeta_{I_v^t}(j) \zeta_{I_v^o}(j)$. $\zeta_{I_v^t}(j)$ *and* $\zeta_{I_v^o}(j)$ *are the Laplace transform of interference* I_v^t *and* I_v^o *and can be formulated as*

$$\zeta_{I_u^t}(j) = \exp\left[-2\lambda_v^t \int_{x_m}^\infty \left(1 - \frac{1}{j p_v h_m x^{\alpha_m} x_i^{-\alpha_m} + \mu} \right) dx_i \right], \tag{12}$$

$$\zeta_{I_{V,o}}(j) = \exp\left[-2\pi\lambda_{va}^t \int_0^\infty \left(1 - \frac{\mu}{j P_v h_m x_i^{-\alpha_m} + \mu} dx_i \right) x dx \right]. \tag{13}$$

In Equation (10), $f_{m,1}(x)$ *is the distance distribution for vehicles in Case 1.* $f_{m,1}(x)$ *is*

$$f_{x_m|1}(x) = \frac{\exp\left(-\lambda_s^t \pi 2 \iota_{m,s}^{-\frac{1}{\alpha_s}} x^{\frac{\alpha_m}{\alpha_s}} \right) f_{x_m}(x)}{\Pr(Case\,1)}, \tag{14}$$

where $\iota_{m,s} = \frac{P_v h_m}{P_v h_s}$, $\Pr(Case\ 1)$ *is the joint association probability of Case 1,* $f_m(x)$ *is the probability density function (PDF) of* x_M. $\Pr(Case\ 1)$ *can be formulated as*

$$\Pr(Case\ 1) = 1 - \int_0^\infty \left[2\lambda_s^t \exp\left(-\lambda_m^t \pi \iota_{m,s}^{\frac{2}{\alpha_m}} x_m^{\frac{2\alpha_S}{\alpha_m}} - 2\lambda_s^t x_s\right)\right] dx_s. \tag{15}$$

According to the null probability of 1-D and 2-D PPPs [29], the PDF of x_M *is*

$$f_m(x_m) = 2\pi x_m \lambda_m^t \exp\left(-\lambda_m^t \pi x_m^2\right). \tag{16}$$

Proof. The proof of joint association probability of Case 1 (UL = MBS, DL = MBS) is

$$\begin{aligned}
&\Pr(Case\,1)\\
&= Pr(\kappa_{m,s} x_m^{-\alpha_m} > x_s^{-\alpha_s})\\
&= E_{x_S}\left[\Pr\left(x_m < \iota_{m,s}^{\frac{1}{\alpha_m}} x_s^{\frac{\alpha_s}{\alpha_m}} | X_s\right)\right]\\
&= \int_0^\infty F_m\left(\iota_{m,s}^{\frac{1}{\alpha_m}} x_s^{\frac{\alpha_s}{\alpha_m}}\right) f_s(x_s) dx_s\\
&\overset{(a)}{=} 1 - \int_0^\infty \left[2\lambda_s^t \exp\left(-\lambda_m^t \pi \iota_{m,s}^{\frac{2}{\alpha_m}} x_s^{\frac{2\alpha_s}{\alpha_m}} - 2\lambda_s^t x_s\right)\right] dx_s,
\end{aligned} \tag{17}$$

where (a) follows from substituting $F_m(\cdot)$ and $f_s(\cdot)$ from the CDF and PDF expressions.

The spectral efficiency derivation follows from:

$$E[\ln(1 + SINR_u)] = \int_0^\infty P[\ln(1 + SINR_u) > t] dt, \tag{18}$$

where $P[\ln(1 + SINR_u) > t]$ is derived using Laplace transform techniques. The proof of $\zeta_{I_u}(j)$ follows from the probability generating functional (PGFL) of 1-D PPP [30]. □

Lemma 2. *The spectral efficiency of DL for Case 1 is formulated as*

$$\tau_d^1 = \int_0^\infty f_{m,1}(x) E[\ln(1 + SINR_d)] dx, \tag{19}$$

where $E[\ln(1 + SINR_d)]$ *is*

$$E[\ln(1 + SINR_d)] = \int_0^\infty e^{-\frac{\left(e^t - 1\right) x^{\alpha_d} \sigma_d^2}{P_m h_m}} \zeta_{I_d}(j) dt, \tag{20}$$

where $j = \frac{\left(e^t - 1\right) x^{\alpha_m}}{P_m h_m}$, $\zeta_{I_d}(j) = \zeta_{I_m}(j) \zeta_{I_s^t}(j) \zeta_{I_s^o}(j)$. $\zeta_{I_m}(j)$, $\zeta_{I_s^t}(j)$, $\zeta_{I_s^o}(j)$ *are*

$$\zeta_{I_m}(j) = \exp\left[-2\pi\lambda_m^t \int_{x_m}^\infty \left(1 - \frac{\mu}{j p_m h_m x_i^{-\alpha_m} + \mu}\right) x_i dx_i\right], \tag{21}$$

$$\zeta_{I_s^t}(j) = \exp\left[-2\lambda_s^t \int_{\iota_{m,s}^{\frac{1}{\alpha_S}} x_m^{\frac{\alpha_m}{\alpha_S}}}^\infty \left(1 - \frac{\mu}{j p_s h_s x_i^{-\alpha_s} + \mu}\right) dx_i\right], \tag{22}$$

$$\zeta_{I_s^o}(j) = \exp\left[-2\pi\lambda_{sa}^t \int_0^\infty \left(1 - \frac{\mu}{j p_s h_s^o x_i^{-\alpha_s} + \mu}\right) x_i dx_i\right]. \tag{23}$$

Proof. The distance distribution $f_{m,1}(x)$ is derived via the CCDF approach. We first compute the conditional CCDF as

$$\begin{aligned} F^{C}_{x_m|1} &= \Pr(x_m > x | \kappa_{m,s} x_m^{-\alpha_m} > x_s^{-\alpha_s}) \\ &= \frac{\Pr(x_m > x; x_s > \iota_{s,m}^{\frac{1}{\alpha_s}} x_m^{\frac{\alpha_m}{\alpha_s}})}{\Pr(Case\,1)} \\ &\overset{(a)}{=} \frac{\int_x^{\infty} \exp\left(-\lambda_s^t \pi 2 \iota_{m,s}^{-\frac{1}{\alpha_s}} x_m^{\frac{\alpha_m}{\alpha_s}}\right) f_{x_m}(x_m) dx_m}{\Pr(Case\,1)}, \end{aligned} \tag{24}$$

where (a) follows from substituting the null probability of the 1-D PPP for x_s. The CDF is $F_{x_m|1} = 1 - F^{C}_{x_m|1}$, and the PDF is obtained by differentiating the CDF: $f_{x_m|1} = dF_{x_m|1}/dx$. The spectral efficiency derivation follows from Equation (18) and the PGFL of PPPs as in Lemma 1. □

Lemma 3. *The spectral efficiency of UL for Case 2 is formulated as*

$$\tau_u^2 = \int_0^{\infty} f_{s,2}(x) E[\ln(1 + SINR_u)] dx, \tag{25}$$

where $f_{s,2}(x)$ is the PDF of UL for Case 2 and can be formulated as

$$\begin{aligned} f_{s,2}(x) = f_{x_s}(x) \Bigg[&\exp\left(-\lambda_m^t \pi \iota_{m,s}^{\frac{2}{\alpha_m}} x^{\frac{\alpha_s}{\alpha_m}}\right) - \\ &\exp\left(-\lambda_m^t \pi \kappa_{m,s}^{\frac{2}{\alpha_m}} x^{\frac{\alpha_s}{\alpha_m}}\right) \Bigg] / \Pr(Case\,2), \end{aligned} \tag{26}$$

where $\Pr(Case\,2)$ is the joint association probability of decoupled access in C-V2X; $f_s(x_s)$ is the distance distribution of x_s as in Equation (27).

$$f_s(x_s) = 2\lambda_s^t \exp(-2\lambda_s^t x_s), \tag{27}$$

$$\begin{aligned} &\Pr(Case\ 2) \\ &= \int_0^{\infty} \left[2\lambda_s^t \exp\left(-\lambda_m^t \pi \iota_{m,s}^{\frac{2}{\alpha_M}} x_S^{\frac{2\alpha_S}{\alpha_M}} - 2\lambda_s^t x_S\right) \right] dx_S \\ &- \int_0^{\infty} \left[2\lambda_s^t \exp\left(-\lambda_M^t \pi \kappa_{m,s}^{\frac{2}{\alpha_M}} x_S^{\frac{2\alpha_S}{\alpha_M}} - 2\lambda_S^t x_S\right) \right] dx_S, \end{aligned} \tag{28}$$

where $\kappa_{m,s} = \frac{P_m h_m}{P_s h_s}$.

In Equation (25), the $E[\ln(1 + SINR_u)]$ is

$$E[\ln(1 + SINR_u)] = \int_0^{\infty} e^{-\frac{\left(e^t - 1\right) x^{\alpha_u} \sigma_u^2}{P_v h_s}} \zeta_{I_u^s}(j) dt, \tag{29}$$

where $j = \frac{\left(e^t - 1\right) x^{\alpha_u}}{P_v h_s}$, $\zeta_{I_u^s}(j) = \zeta_{I_u^t}(j) \times \zeta_{I_u^0}(j)$ and $\zeta_{I_u^t}(j)$, $\zeta_{I_u^0}(j)$ can be formulated as

$$\zeta_{I_u^t}(j) = \exp\left[-2\lambda_v^t \int_{x_s}^{\infty} \left(1 - \frac{\mu}{(e^t - 1) x^{\alpha_u} x_i^{-\alpha_u} + \mu} \right) dx_i \right], \tag{30}$$

$$\zeta_{I_u^o}(j) = \exp\left[-2\pi\lambda_{va}^t \int_0^\infty \left(1 - \frac{\mu}{jp_v h_v^o x_i^{-\alpha_s} + \mu}\right) x_i dx_i\right], \tag{31}$$

where $\lambda_{va}^t = \lambda_v^t \lambda_l$.

Proof. The proof of joint association probability of Case 2 (UL = SBS, DL = MBS) is

$$\begin{aligned}
&\Pr(Case\,2)\\
&\overset{(a)}{=} \Pr\left(x_m < \kappa_{m,s}^{\frac{1}{\alpha_m}} x_s^{\frac{\alpha_s}{\alpha_m}}\right) - \Pr\left(x_m < \iota_{m,s}^{\frac{1}{\alpha_m}} x_s^{\frac{\alpha_s}{\alpha_m}}\right)\\
&\overset{(b)}{=} E_{x_s}\left[\Pr\left(x_m < \kappa_{m,s}^{\frac{1}{\alpha_m}} X_S^{\frac{\alpha_S}{\alpha_M}} | x_S\right)\right] - E_{x_s}\left[\Pr\left(x_m < \iota_{m,s}^{\frac{1}{\alpha_M}} X_S^{\frac{\alpha_s}{\alpha_m}} | x_s\right)\right],
\end{aligned} \tag{32}$$

where (a) converts the probability expression, and (b) derives the expectations for X_s. The remaining derivations follow similar steps as in Lemma 1. The spectral efficiency derivation follows the same approach as Lemma 1. □

Lemma 4. *The spectral efficiency of DL for Case 2 is formulated as*

$$\tau_d^2 = \int_0^\infty f_{m,2}(x) E[\ln(1 + SINR_d)] dx, \tag{33}$$

where $f_{m,2}(x)$ *is the PDF of DL for Case 2 and can be formulated as*

$$\begin{aligned}
f_{m,2}(x) =& f_{x_m}(x)\left[\exp\left(-\lambda_s^t \pi 2\kappa_{m,s}^{-\frac{1}{\alpha_s}} x^{\frac{\alpha_m}{\alpha_s}}\right) - \right.\\
&\left.\exp\left(-\lambda_s^t \pi 2\iota_{m,s}^{-\frac{1}{\alpha_S}} x^{\frac{\alpha_m}{\alpha_s}}\right)\right] / \Pr(Case1),
\end{aligned} \tag{34}$$

where $E[\ln(1 + SINR_d)]$ *is*

$$E[\ln(1 + SINR_d)] = \int_0^\infty e^{-\frac{\left(e^t - 1\right) x^{\alpha_d} \sigma_d^2}{P_m h_m}} \zeta_{I_d}(j) dt, \tag{35}$$

where $j = \frac{\left(e^t - 1\right) x^{\alpha_d}}{P_m h_m}$, $\zeta_{I_d}(j) = \zeta_{I_m}(j)\zeta_{I_s^t}(j)\zeta_{I_s^o}(j)$, $\zeta_{I_m}(j)$. $\zeta_{I_s^t}(j)$, $\zeta_{I_s^o}(j)$ *are*

$$\zeta_{I_m}(j) = \exp\left[-2\pi\lambda_m^t \int_{x_m}^\infty \left(1 - \frac{\mu}{jp_m h_m x_i^{-\alpha_d} + \mu}\right) x_i dx_i\right], \tag{36}$$

$$\zeta_{I_s^t}(j) = \exp\left[-2\lambda_s^t \int_{\kappa_{s,m}^{\frac{1}{\alpha_s}} x_m^{\frac{\alpha_m}{\alpha_s}}}^{\iota_{s,m}^{\frac{1}{\alpha_s}} x_m^{\frac{\alpha_m}{\alpha_s}}} \left(1 - \frac{\mu}{jp_s h_s x_i^{-\alpha_s} + \mu}\right) dx_i\right], \tag{37}$$

$$\zeta_{I_s^o}(j) = \exp\left[-2\pi\lambda_{sa}^t \int_0^\infty \left(1 - \frac{\mu}{jp_s h_s^o x_i^{-\alpha_d} + \mu}\right) x_i dx_i\right], \tag{38}$$

where $f_{m,2}(x)$, $f_{s,1}(x)$ *is the joint distance distribution for Case 2 in DL and can be calculated as in Equation* (39) *as*

$$f_{m,2}(x) = f_{x_m}(x)\left[\exp\left(-\lambda_s^t \pi 2\kappa_{s,m}^{\frac{1}{\alpha_s}} x^{\frac{\alpha_m}{\alpha_s}}\right) - \exp\left(-\lambda_s^t \pi 2\iota_{s,m}^{\frac{1}{\alpha_s}} x^{\frac{\alpha_m}{\alpha_s}}\right)\right] / \Pr(Case1), \tag{39}$$

Proof. The distance distribution $f_{m,2}(x)$ for DL in Case 2 is derived via the CCDF approach. We compute the conditional CCDF as

$$\begin{aligned} F^C_{x_m|2} &= \Pr(x_m > x | \iota_{m,s} x_m^{-\alpha_m} < x_s^{-\alpha_s} < \kappa_{m,s} x_m^{-\alpha_m}) \\ &= \frac{\Pr(x_m > x; \iota_{s,m}^{\frac{1}{\alpha_s}} x_m^{\frac{\alpha_m}{\alpha_s}} < x_s < \kappa_{s,m}^{\frac{1}{\alpha_s}} x_m^{\frac{\alpha_m}{\alpha_s}})}{\Pr(Case\,2)} \\ &\overset{(a)}{=} \frac{\int_x^\infty \left[\exp\left(-\lambda_s^t \pi 2\iota_{m,s}^{-\frac{1}{\alpha_s}} x_m^{\frac{\alpha_m}{\alpha_s}}\right) - \exp\left(-\lambda_s^t \pi 2\kappa_{m,s}^{-\frac{1}{\alpha_s}} x_m^{\frac{\alpha_m}{\alpha_s}}\right)\right] f_{x_m}(x_m) dx_m}{\Pr(Case\,2)}, \end{aligned} \tag{40}$$

where (a) follows from the difference of two null probabilities of the 1-D PPP for x_s. The CDF is $F_{x_m|2} = 1 - F^C_{x_m|2}$, and the PDF is obtained by differentiating: $f_{x_m|2} = dF_{x_m|2}/dx$. The spectral efficiency derivation follows from Equation (18) and the PGFL of PPPs. □

Lemma 5. *The spectral efficiency of UL for Case 3 is formulated as*

$$\tau_u^3 = \int_0^\infty f_{s,3}(x) E[\ln(1 + SINR_u)] dx, \tag{41}$$

where $f_{s,3}(x)$ is the joint distance distribution of Case 3 and $f_{s,3}(x)$ is formulated as in (42).

$$f_{x_s|Case\,3} = \frac{\exp\left(-\lambda_m^t \pi \kappa_{m,s}^{\frac{2}{\alpha_m}} x^{\frac{2\alpha_s}{\alpha_m}}\right) f_{x_s}(x)}{\Pr(Case\,3)}. \tag{42}$$

$E[\ln(1 + SINR_d)]$ *is*

$$E[\ln(1 + SINR_u)] = \int_0^\infty e^{-\frac{\left(e^t - 1\right) x^{\alpha_s} \sigma_u^2}{P_v}} \zeta_{I_u}(j) dt, \tag{43}$$

where $j = \frac{\left(e^t - 1\right) x^{\alpha_s}}{P_v h_s}$, $\Pr(Case\,3)$ is the joint association probability of Case 3 and is formulated as

$$\Pr(Case\,3) = \int_0^\infty \left[2\lambda_s^t \exp\left(-\lambda_m^t \pi \kappa_{m,s}^{\frac{2}{\alpha_m}} x_s^{\frac{2\alpha_s}{\alpha_m}} - 2\lambda_s^t x_s\right)\right] dx_s. \tag{44}$$

$\zeta_{I_u}(j) = \zeta_{I_v^t}(j) \times \zeta_{I_v^o}(j)$ and $\zeta_{I_u^t}(j)$, $\zeta_{I_u^o}(j)$ can be formulated as

$$\zeta_{I_v^t}(j) = \exp\left[-2\lambda_v^t \int_{x_s}^\infty \left(1 - \frac{\mu}{jP_v h_s x_i^{-\alpha_s} + \mu}\right) dx_i\right], \tag{45}$$

$$\zeta_{I_{v,o}}(j) \overset{(a)}{=} \exp\left[-2\pi\lambda_{va}^t \int_0^\infty \left(1 - \frac{\mu}{jP_v h_s^o x_i^{-\alpha_s} + \mu} dx_i\right) x dx\right]. \tag{46}$$

Proof. The proof of joint association probability of Case 3 (UL = SBS, DL = SBS) is

$$\begin{aligned}
&\Pr(Case\,3)\\
&= \Pr\left(x_s^{-\alpha_s} > \kappa_{m,s} x_m^{-\alpha_m}\right)\\
&\overset{(a)}{=} 1 - \Pr(x_m < \kappa_{m,s}^{\frac{1}{\alpha_m}} x_s^{\frac{\alpha_s}{\alpha_m}})\\
&\overset{(b)}{=} \int_0^\infty \left[2\lambda_s^t \exp\left(-\lambda_m^t \pi \kappa_{m,s}^{\frac{2}{\alpha_m}} x_s^{\frac{2\alpha_s}{\alpha_m}} - 2\lambda_s^t x_s\right)\right] dx_s,
\end{aligned} \tag{47}$$

where (a) calculates the probability of its complement, and (b) follows the steps as in Lemma 1. The spectral efficiency derivation follows the same approach as Lemma 1. □

Lemma 6. *The spectral efficiency of DL for Case 3 is*

$$\tau_d^3 = \int_0^\infty f_{s,3}(x) E[\ln(1 + SINR_d)] dx, \tag{48}$$

where $E[\ln(1 + SINR_d)]$ *is*

$$E[\ln(1 + SINR_d)] = \int_0^\infty e^{-\frac{\left(e^t - 1\right) x^{\alpha_s} \sigma_d^2}{P_s h_s}} \zeta_{I_d}(j) dt, \tag{49}$$

where $j = \frac{\left(e^t - 1\right) x^{\alpha_s}}{P_s h_s}$, $I_d = I_m + I_s^o + I_s^t$*the* $\zeta_{I_d^c}(j)$ *is*

$$\zeta_{I_m}(j) = \exp\left[-2\pi\lambda_m^t \int_{\kappa_{m,s}^{\frac{1}{\alpha_m}} x_s^{\frac{\alpha_s}{\alpha_m}}}^\infty \left(1 - \frac{\mu}{j p_m h_m x_i^{-\alpha_m} + \mu}\right) x_i dx_i\right], \tag{50}$$

$$\zeta_{I_s^t}(j) = \exp\left[-2\lambda_s^t \int_{x_s}^\infty \left(1 - \frac{\mu}{j p_s h_s x_i^{-\alpha_s} + \mu}\right) dx_i\right], \tag{51}$$

$$\zeta_{I_s^o}(j) = \exp\left[-2\pi\lambda_{sa}^t \int_0^\infty \left(1 - \frac{\mu}{j p_s h_s^o x_i^{-\alpha_d} + \mu}\right) x_i dx_i\right]. \tag{52}$$

Proof. The distance distribution $f_{s,3}(x)$ for DL in Case 3 is derived via the CCDF approach. We compute the conditional CCDF as

$$\begin{aligned}
F_{x_s|3}^C &= \Pr(x_s > x | x_s^{-\alpha_s} > \kappa_{m,s} x_m^{-\alpha_m})\\
&= \frac{\Pr(x_s > x; x_m > \kappa_{m,s}^{\frac{1}{\alpha_m}} x_s^{\frac{\alpha_s}{\alpha_m}})}{\Pr(Case\,3)}\\
&\overset{(a)}{=} \frac{\int_x^\infty \exp\left(-\lambda_m^t \pi \kappa_{m,s}^{\frac{2}{\alpha_m}} x_s^{\frac{2\alpha_s}{\alpha_m}}\right) f_{x_s}(x_s) dx_s}{\Pr(Case\,3)},
\end{aligned} \tag{53}$$

where (a) follows from substituting the null probability of the 2-D PPP for x_m. The CDF is $F_{x_s|3} = 1 - F_{x_s|3}^C$, and the PDF is obtained by differentiating $f_{x_s|3} = dF_{x_s|3}/dx$. The spectral efficiency derivation follows from Equation (18) and the PGFL of PPPs. □

Proof. The spectral efficiency expressions from Lemma 1 to Lemma 6 are obtained by following the Laplace transform approach outlined in the proof of Lemma 1, where the key steps are: converting the expectation of the logarithmic SINR function to an integral via the

identity $E[\ln(1+\mathrm{SINR})] = \int_0^\infty \Pr[\ln(1+\mathrm{SINR}) > t]dt$, decomposing the interference Laplace transform using the PGFL of PPPs, and evaluating the resulting integrals numerically. □

Therefore, the average spectral efficiency of Case r can be calculated as

$$\tau_r = B_r(x_u\tau_u^r + x_d\tau_d^r), \tag{54}$$

where B_r is the bandwidth allocated to Case r, $r \in \{1,2,3\}$ by WSP n, x_u, x_d is the allocation ratio of UL and DL bandwidth and here we set x_u and x_d to 0.2 and 0.8, respectively [31].

4.3. Evolution Game Scheme

In UL/DL decoupled access C-V2X, we denote the set of WSPs as $\aleph = \{1,2,\ldots,n\}$, and every WSP n may provide different services $\mathrm{Y} = \{1,2,\ldots,r\}$, i.e., the three types of decoupled access in this paper, to vehicles. The WSPs have bandwidth allocation profiles $B = \{B_1, B_2, \ldots, B_n\}, B_n = (B_{n,r})_{r\in\mathrm{Y}}$ for services. Each vehicle can charge price $C_{n,r}$ for service r provided by WSP n. Thus, we use $x_{n,r}, \sum_{n\in\aleph} x_{n,r} = 1$ to denote the population distribution caused by vehicles choosing different services r according to rate and cost. Thus, based on the results of Section II, the expected average user rate is

$$\bar{R}_{r,v} = \frac{B_r\tau_r}{N_r}, N_r = x_r Pr(Case\, r)\lambda_v^t, \tag{55}$$

where N_r is the average vehicle number of service r, and x_r is the probability of the vehicle choosing WSP n for service r.

To reach the evolutionary equilibrium, we propose an iterative algorithm based on the pairwise proportional imitation rule. The algorithm starts with an even distribution of vehicles across WSPs and iteratively updates vehicle strategies based on payoff comparisons. In each iteration, vehicles with below-average payoff have the opportunity to switch to strategies with higher payoff, with the switching probability proportional to the payoff difference. This process continues until all vehicles achieve the same payoff, indicating that the evolutionary equilibrium has been reached. Note that each vehicle only needs to compare its own payoff with the population average payoff, which is broadcast by the serving WSP, rather than requiring global knowledge of all individual payoffs. The detailed procedure is presented in Algorithm 1.

Algorithm 1: Evolutionary Game of WSP Selection

Input: $C_{a_p,r}$, τ_r, $B_{a_p,r}$;
Initialize: Allocate vehicles to WSPs evenly, obtain Xx;
repeat
  Obtain each vehicle's payoff π_{a_p} **by Equation** (56);
  Calculate the average payoff $\bar{\pi}$ **by Equation** (57);
  for $v \in \omega_{v,o}^t$ **do**
    Generate a random number $\varepsilon \in (0,1)$;
    if $\pi_{a_p} < \bar{\pi}$ **then**
      if $\varepsilon < (\bar{\pi} - \pi_{a_p})/\bar{\pi}$ **then**
        vehicle v **chooses a strategy with higher payoff, update X;**
      end
    end
  end
until $\pi_{a_p} = \bar{\pi}$;
Output: π_{a_p}, **X;**

The computational complexity of Algorithm 1 is $O(T \cdot |\varpi_v^t| \cdot p)$, where T is the number of iterations until convergence, $|\varpi_v^t|$ is the number of vehicles, and p is the number of populations.

For the evolution game scheme, we formulate the following definition:

- Population: The vehicles that choose the same service r is referred to as a population, thus there are p populations and we use $\Psi = \{1, 2, \ldots, p\}$ to denote the population set.
- Strategy space: The vehicle in p-th population can decide which WSP to access, thus the strategy space can be expressed as $\Theta_p = \{n | n \in \aleph, p \in \Psi_n\}$.
- Population state: x_{a_p} is the proportion of vehicles choosing strategy $a_p \in \Theta_p$, and $\sum_{a_p \in \Theta_p} x_{a_p} = 1$. Thus, all strategies are set as a population state $\mathbf{x_p} = (x_{a_p})_{a_p \in \Theta_p}$. For all populations, $\mathbf{X} = \{\mathbf{x_1}, \mathbf{x_2}, \ldots, \mathbf{x_p}\}$.
- Payoff function: We use a logarithmic function to evaluate the satisfaction level of the strategy a_p as

$$\pi_{a_p} = ln(1 + \frac{\bar{R}_{a_p,r}}{C_{a_p,r}}) = ln(1 + \frac{\zeta_{a_p,r}\tau_r}{x_{a_p}}), \tag{56}$$

  where $\zeta_{a_p,r} = \frac{B_{a_p,r}}{C_{a_p,r} Pr(Case\, i) \lambda_v^t}$. The logarithmic form captures the diminishing return of user satisfaction with respect to the rate–cost ratio and can be extended to support differentiated vehicle preferences by introducing type-specific weight parameters. Then the average payoff of vehicles is

$$\bar{\pi} = \frac{\sum_{i \in \varpi_{v,o}^t} \pi_i}{\left\| \varpi_{v,o}^t \right\|}, \tag{57}$$

  where $\left\| \varpi_v^t \right\|$ is the number of vehicles in ϖ_v^t.

In Equation (56), it can be found that the vehicle's actual payoff depends not only on its chosen strategy for the WSP but also on the proportion of other vehicles who choose the same WSP (i.e., the behavior of other vehicles). When the WSP's spectrum allocation strategy remains unchanged, as x_{a_p} increases, the payoff of vehicles under this strategy decreases. Thus, we design an evolutionary game algorithm based on service cost for vehicles to select WSP as shown in Algorithm 1.

4.4. Bandwidth Allocation Game

After analyzing the evolutionary equilibrium of vehicle WSP selection, we now investigate the bandwidth allocation problem for WSPs. Each WSP aims to maximize its revenue by optimally allocating bandwidth to different services while considering the competition from other WSPs and the reaction of vehicles. The service price $C_{n,r}$ is a parameter that reflects the market condition and can be configured by the WSPs. In the following, we focus on the bandwidth allocation strategy given the price configuration.

4.4.1. Revenue Function

The revenue of WSP n is determined by the number of vehicles it serves and the prices it charges. Given the bandwidth allocation profile $B_n = (B_{n,1}, B_{n,2}, B_{n,3})$ and the population distribution $x_{n,r}$, the revenue function of WSP n can be expressed as:

$$U_n(B_n, B_{-n}) = \sum_{r=1}^{3} x_{n,r} \lambda_v^t \Pr(Case\, r) C_{n,r}, \tag{58}$$

where B_{-n} denotes the bandwidth allocation strategies of all WSPs except WSP n.

4.4.2. Optimization Problem

The bandwidth allocation problem for WSP n can be formulated as:

$$\begin{aligned} \max_{B_n} \quad & U_n(B_n, B_{-n}) \\ \text{s.t.} \quad & \sum_{r=1}^{3} B_{n,r} = B_n^{total}, \\ & B_{n,r} \geq 0, \quad \forall r \in \{1,2,3\}, \end{aligned} \tag{59}$$

where B_n^{total} is the total bandwidth available to WSP n.

To solve this optimization problem, we introduce the cost performance index per unit bandwidth:

$$\eta_{n,r} = \frac{\tau_r}{C_{n,r} \Pr(Case\, r) \lambda_v^t}. \tag{60}$$

Using the Lagrange multiplier method, the optimal bandwidth allocation for WSP n can be obtained by solving:

$$B_{n,r}^* = \sqrt{\frac{\lambda_v^t C_{n,r} X_{n,r}}{\mu_n \eta_{n,r}}} - \frac{X_{n,r}}{\eta_{n,r}}, \tag{61}$$

where $X_{n,r} = \sum_{i \neq n} \eta_{i,r} B_{i,r}$ represents the influence from other WSPs, and μ_n is the Lagrange multiplier satisfying $\sum_{r=1}^{3} B_{n,r}^* = B_n^{total}$.

4.4.3. Bandwidth Allocation Algorithm

Based on the above analysis, we propose an iterative algorithm to reach the Nash equilibrium of the bandwidth allocation game. The algorithm operates in a distributed manner where each WSP updates its bandwidth allocation strategy based on the current strategies of other WSPs. In each iteration, WSPs first calculate the cost performance index for each service, then compute the influence from competing WSPs, and finally update their bandwidth allocation by solving for the Lagrange multiplier that satisfies the total bandwidth constraint. This iterative process continues until convergence, where no WSP can improve its revenue by unilaterally changing its bandwidth allocation. The convergence to Nash equilibrium is guaranteed by the contraction property of the best response mapping, as established in Theorem 1. The detailed procedure is presented in Algorithm 2.

4.4.4. Uniqueness of Nash Equilibrium

To guarantee the uniqueness of the Nash equilibrium in the bandwidth allocation game, we provide the following analysis based on contraction mapping theory.

Lemma 7. *If the best response mapping is a contraction on the whole strategy space, there exists a unique Nash equilibrium in the game. A mapping $f(x)$ is a contraction if and only if $\|f(x_1) - f(x_2)\| \leq \alpha \|x_1 - x_2\|$, $\forall x_1, x_2$, where $0 < \alpha < 1$ and $\|\cdot\|$ denotes a proper norm.*

Theorem 1. *When all WSPs provide the same set of services $\{1,2,3\}$, if for any WSP n, the following condition holds:*

$$\left\| \frac{\partial \chi_n}{\partial B_{-n}} \right\| < 1, \tag{62}$$

where χ_n is the best response function of WSP n and B_{-n} represents the bandwidth allocation of other WSPs, then the Nash equilibrium of the bandwidth allocation game is unique.

Algorithm 2: Bandwidth Allocation Algorithm for WSPs

Input: $C_{n,r}$, τ_r, $\Pr(Case\, r)$, λ_v^t, B_n^{total};
Initialize: Randomly allocate bandwidth $B_{n,r}^{(0)}$ **for all** n, r, $t = 0$;
repeat
  for *each WSP n and service r* **do**
    Calculate cost performance index:
    $\eta_{n,r} = \frac{\tau_r}{C_{n,r} \Pr(Case\, r) \lambda_v^t}$;
  end
  for *each WSP n and service r* **do**
    Calculate influence from other WSPs:
    $X_{n,r} = \sum_{i=1}^{3} \eta_{i,r} B_{i,r}^{(t)} - \eta_{n,r} B_{n,r}^{(t)}$;
  end
  for *each WSP n* **do**
    Solve for Lagrange multiplier μ_n **such that:**
    $\sum_{r=1}^{3} \left[\sqrt{\frac{\lambda_v^t C_{n,r} X_{n,r}}{\mu_n \eta_{n,r}}} - \frac{X_{n,r}}{\eta_{n,r}} \right] = B_n^{total}$;
    for *each service r* **do**
      Update: $B_{n,r}^{(t+1)} = \sqrt{\frac{\lambda_v^t C_{n,r} X_{n,r}}{\mu_n \eta_{n,r}}} - \frac{X_{n,r}}{\eta_{n,r}}$;
    end
  end
  $t = t + 1$;
until *convergence*;
Output: Nash equilibrium bandwidth allocation $B_{n,r}^*$;

Proof. The best response function $\chi_n(B_{-n})$ for WSP n is given by the solution to the optimization problem. For any two bandwidth allocation profiles B_{-n} and $\tilde{B}_{-n}$, we define $\Gamma_n(\tau) = \chi_n(\tilde{B}_{-n} + \tau(B_{-n} - \tilde{B}_{-n}))$.

By the chain rule:

$$\frac{\partial \Gamma_n(\tau)}{\partial \tau} = (B_{-n} - \tilde{B}_{-n})^T \frac{\partial \chi_n}{\partial B_{-n}}. \tag{63}$$

Integrating from $\tau = 0$ to $\tau = 1$:

$$\chi_n(B_{-n}) - \chi_n(\tilde{B}_{-n}) = \int_0^1 (B_{-n} - \tilde{B}_{-n})^T \frac{\partial \chi_n}{\partial B_{-n}} d\tau. \tag{64}$$

Taking norms on both sides:

$$\|\chi_n(B_{-n}) - \chi_n(\tilde{B}_{-n})\| \leq \left\| \frac{\partial \chi_n}{\partial B_{-n}} \right\| \|B_{-n} - \tilde{B}_{-n}\|. \tag{65}$$

When $\| \frac{\partial \chi_n}{\partial B_{-n}} \| < 1$, the best response mapping is a contraction. By Lemma 7, the Nash equilibrium is unique. □

The condition in Theorem 1 can be verified numerically for specific network parameters. When the uniqueness condition is satisfied, Algorithm 2 converges to the same Nash equilibrium regardless of the initial bandwidth allocation.

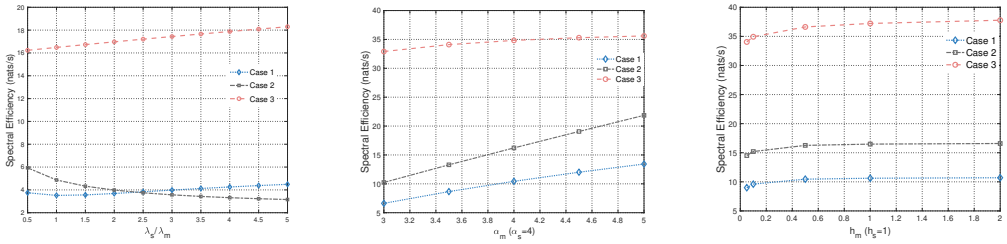
5. Simulation Results

We simulate the proposed analysis in multiple WSPs UL/DL decoupled access C-V2X, which consists of three services (i.e., Case 1, Case 2, and Case 3), three WSPs, and 3000 vehicles as shown in Figure 1. The detailed channel parameters and simulation setting are listed in Table 1 [9,32].

Table 1. Main parameters.

Channel Parameters	**Value**
MBS transmitting power P_m (dBm)	46
SBS transmitting power P_s (dBm)	23
Vehicle transmitting power P_v (dBm)	20
The densities of vehicles, MBSs, and SBSs (nodes/km)	15, 0.5, 2
The densities of lines	$10/\pi$
The channel gains h_m, h_s	0.1, 1
Path loss exponent $\alpha_m = \alpha_s$	2.5
Mean of log-normal shadowing gain (db)	0
Std deviation of log-normal shadowing gain (dB)	4
Rayleigh fading parameter μ	1
Simulation parameters	**Value**
Bandwidth allocated by WSP 1 to Cases 1, 2, 3 (MHz)	[5 2 3]
Bandwidth allocated by WSP 2 to Cases 1, 2, 3 (MHz)	[2 3 5]
Bandwidth allocated by WSP 3 to Cases 1, 2, 3 (MHz)	[4 2 4]
Cost charged by WSPs to Cases 1, 2, 3 ($)	[2 3 5]
The number of vehicles	3000

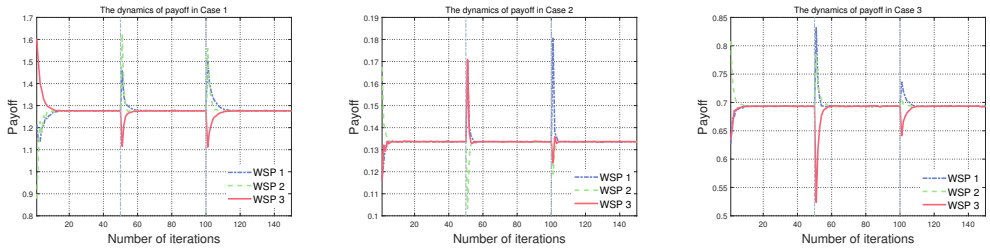
Figure 2 depicts the average rate for three decoupled access services. It can be observed that the average rate in Case 3 is higher than that of Case 1 and Case 2. This is mainly because Case 3 utilizes SBSs for both UL and DL, and with a larger number of SBSs deployed, the SBSs are closer to the vehicles compared to MBSs, which compensates for the disadvantage of lower transmit power. Case 1 shows a moderate performance as it uses MBSs for both UL and DL, benefiting from higher transmit power but suffering from longer distances. Case 2 exhibits the lowest rate because the hybrid configuration (MBS for DL and SBS for UL) creates an imbalance in link quality, where the DL from the distant MBS becomes the bottleneck despite the good UL performance from the nearby SBS. Furthermore, Figure 2b shows the spectral efficiency versus α_m with fixed $\alpha_s = 4$. An interesting observation is that the spectral efficiency of all three cases increases with α_m. This is because in interference-limited networks, a larger path loss exponent causes the aggregate interference from distant MBSs to decay faster than the desired signal from the serving MBS, resulting in improved SINR. Case 3 remains relatively stable since its link quality is dominated by an SBS with fixed $\alpha_s = 4$, while Cases 1 and 2 show significant improvement as the MBS interference diminishes. Case 3 consistently outperforms Cases 1 and 2 across all α_m values, confirming that the advantage of Case 3 is a joint effect of network density and propagation environment, not merely a density effect. To examine the robustness of the case ranking with respect to the MBS-SBS gain gap, we vary h_m from 0.05 to 2.0 with fixed $h_s = 1$ and plot the spectral efficiency in Figure 2c. Across all tested values, the ranking Case 3 > Case 2 > Case 1 remains unchanged. As h_m increases, Cases 1 and 2 benefit from the improved MBS link quality, while Case 3 gains moderately since both UL and DL rely on SBSs. The consistent ranking confirms that the superiority of Case 3 is robust to the assumed gain gap between MBS and SBS links.



(a) Weighted spectral efficiency versus λ_s/λ_m **(b)** Spectral efficiency versus α_m ($\alpha_s = 4$) **(c)** Spectral efficiency versus h_m ($h_s = 1$)

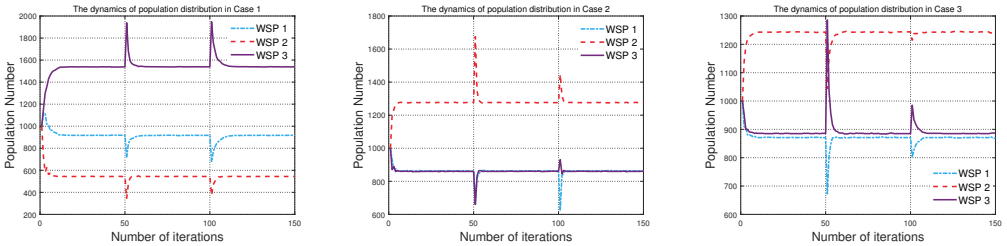
Figure 2. (**a**) The average rates for UL/DL decoupled access and coupled access ($B_u = 2.5$ MHz, $B_d = 10$ MHz). (**b**) Spectral efficiency versus MBS path loss exponent α_m ($\alpha_s = 4$). (**c**) Spectral efficiency versus MBS channel gain h_m ($h_s = 1$).

We randomly assign 3000 vehicles evenly to three services. Subsequently, the vehicles are subjected to pairwise proportional imitation based on their individual needs, rates, and the service costs provided by the WSPs, in the proposed evolutionary game. The payoff distribution and population distribution are shown in Figures 3 and 4. It can be seen that the evolutionary equilibrium of this evolutionary game can be reached in less than 20 iterations. To further observe the asymptotic stability and uniqueness of the evolutionary equilibrium, we introduce two perturbations at the 50th and 100th iterations by randomly changing the selection strategy for some vehicles. After a significant perturbation, it can be observed that the evolutionary game reaches the same equilibrium state as before the perturbation, with the same population distribution and payoff. Additional iterations are required to restore the equilibrium state because of the larger disturbance. The above results indicate that the evolutionary game framework proposed in this paper has excellent stability and rapid evolutionary convergence.



(a) **(b)** **(c)**

Figure 3. The payoff of vehicles choosing the same service in different WSPs. (**a**) The dynamics of payoff in Case 1. (**b**) The dynamics of payoff in Case 2. (**c**) The dynamics of payoff in Case 3.



(a) $\{B_{1,1}, B_{2,1}, B_{3,1}\} = \{5, 2, 4\}$ **(b)** $\{B_{1,2}, B_{2,2}, B_{3,2}\} = \{2, 3, 2\}$ **(c)** $\{B_{1,3}, B_{2,3}, B_{3,3}\} = \{3, 5, 4\}$

Figure 4. The population distribution of vehicles choosing the same service in different WSPs.

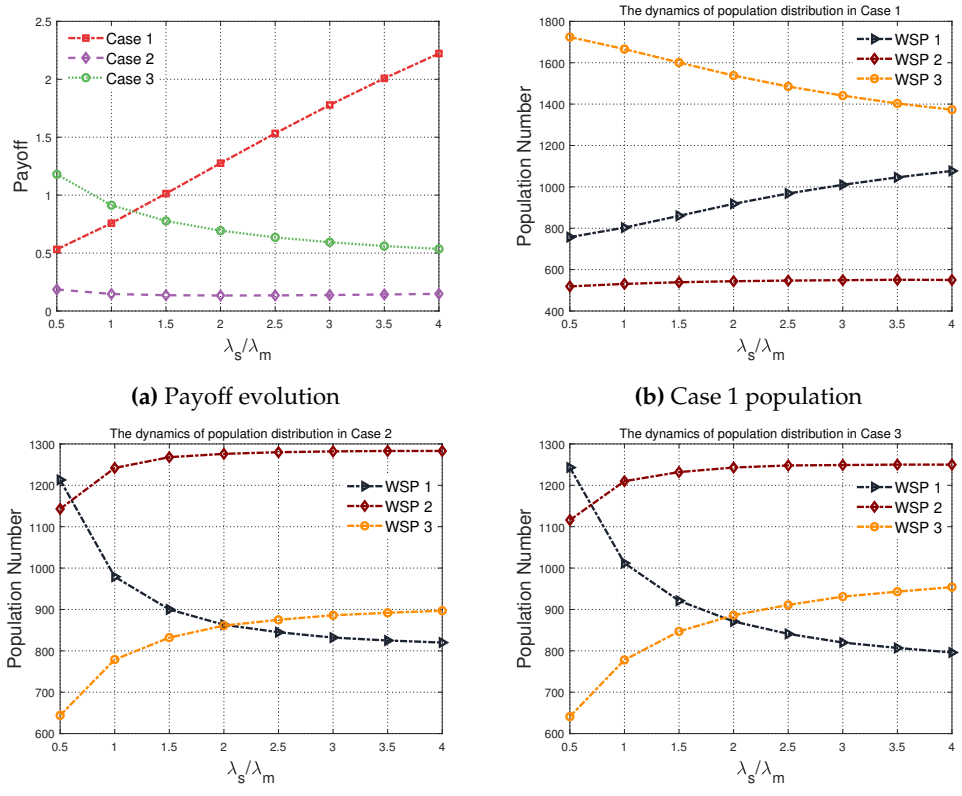
Figure 4 illustrates the evolutionary process of vehicle users selecting different WSPs under three services. Different WSPs have different focuses for various services; hence in

this paper, the characteristic is reflected by setting different bandwidths provided by the WSPs for different services. In Figure 4b,c, the number of vehicles choosing WSP 1 is very small. In Figure 4a, due to WSP 1's emphasis on Case 1, the number of vehicles choosing WSP 1 has increased. In Case 2 and Case 3, because WSP 2 places more emphasis on these two services, the number of vehicles is relatively higher. Due to WSP 3's focus on Case 1, more vehicles are choosing WSP 3 for the Case 1 service. It can be observed that by altering the number of vehicles associated with different WSPs, the evolutionary process quickly converges and restores the unique evolutionary equilibrium.

In Figure 3, WSPs ultimately all achieve the same payoff at evolutionary equilibrium for each service. The payoff for Case 3 is the highest among the three cases. This is because Case 3 can provide high communication rates due to the proximity of SBSs to vehicles, and the cost-effectiveness ratio is favorable. Case 1 achieves moderate payoff as it benefits from higher transmit power but suffers from longer distances to vehicles. Case 2 shows the lowest payoff, mainly because the DL from distant MBSs limits the overall performance despite good UL quality from nearby SBSs, resulting in a poor cost-effectiveness ratio.

5.1. Impact of BS Density on System Performance

To investigate the impact of network density on the evolutionary game and bandwidth allocation, we vary the ratio of SBS density to MBS density and observe the system behavior. Figure 5 shows the evolution of payoff and population distribution under different density ratios.



(a) Payoff evolution

(b) Case 1 population

(c) Case 2 population

(d) Case 3 population

Figure 5. Evolution of payoff and population distribution under different SBS/MBS density ratios.

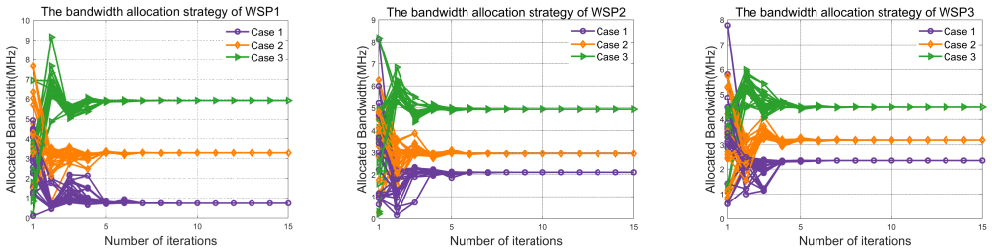
Figure 5 demonstrates the impact of varying SBS/MBS density ratios on the evolutionary game dynamics. Case 1 shows payoff improvement despite not directly benefiting from SBS densification. This occurs because as SBS density increases, vehicles migrate from Case 1 to Cases 2 and 3, reducing competition and congestion in Case 1. During this

analysis, the bandwidth allocation of each WSP is fixed. Therefore, fewer users in Case 1 lead to more bandwidth per remaining user and thus a higher payoff.

Figure 5b–d show how vehicles redistribute among different WSPs under varying SBS/MBS density ratios for each case. Note that the total number of vehicles in each case remains constant at 3000, but their WSP selection changes with network density. In Figure 5b, for Case 1 service, as SBS density increases, vehicles selecting WSP 3 decrease significantly. This is because WSP 3 allocates relatively less bandwidth to Case 1, showing insufficient emphasis on this service type, making it less competitive as network conditions improve. In Figure 5c, for Case 2 service, vehicles selecting WSP 1 show notable decline as SBS density increases. This occurs because increased SBS density significantly improves the cost–performance ratio of Case 2, while WSP 1 allocates the least bandwidth (2 MHz) to Case 2, demonstrating low priority for this service. The combination of improved service quality and insufficient bandwidth allocation makes WSP 1 increasingly unattractive. In Figure 5d, for Case 3 service, WSP 1 experiences the most dramatic population decrease. As SBS density increases, Case 3 achieves substantially higher spectral efficiency and cost–performance ratio. However, WSP 1's relatively low bandwidth allocation to Case 3 indicates insufficient emphasis on this high-performance service, causing vehicles to rapidly migrate toward WSP 2 and WSP 3, which allocate more resources to capitalize on the improved Case 3 performance.

5.2. Bandwidth Allocation Results

Figure 6 illustrates the bandwidth allocation evolution process for the three WSPs. Each WSP starts with a random initial bandwidth allocation and iteratively updates its strategy based on the Nash equilibrium solution. All three WSPs converge to stable bandwidth allocations within 10 iterations, demonstrating fast convergence and the uniqueness of Nash equilibrium.



(a) WSP 1 **(b)** WSP 2 **(c)** WSP 3

Figure 6. Bandwidth allocation strategies of three WSPs converging to Nash equilibrium.

At equilibrium, all three WSPs exhibit a similar pattern: allocating the most bandwidth to Case 3, moderate bandwidth to Case 2, and the least to Case 1. This allocation strategy reflects the trade-off between the inherent performance characteristics and the cost structure of the three cases. Case 3 receives the highest bandwidth allocation because, despite its moderate cost, it offers a balanced performance that maximizes utility without the extreme cost of pure SBS solutions. Case 2 receives a moderate bandwidth allocation, balancing its low cost with its lower performance. Case 1 receives the least bandwidth across all WSPs, indicating that the high service cost outweighs the benefit of high communication rates in this specific equilibrium, making it the least attractive option for large-scale resource allocation. The differentiation among WSPs lies in the degree of allocation: WSP 1 shows the strongest preference for Case 3, WSP 3 prioritizes Case 1, while WSP 2 maintains a more balanced approach between Case 3 and Case 1.

6. Conclusions

This paper investigates the performance analysis and WSP selection problem in UL/DL decoupled access C-V2X networks. We derive tractable spectral efficiency expressions for both UL and DL using stochastic geometry, considering three decoupled access cases. A hierarchical game framework is proposed, combining evolutionary game for vehicle WSP selection and non-cooperative game for WSP bandwidth allocation. The uniqueness of Nash equilibrium is proved based on contraction mapping theory. Extensive simulations validate the analytical results and demonstrate the convergence and stability of the proposed framework. The results show that the evolutionary equilibrium can be reached within 20 iterations and remains stable under perturbations, and the bandwidth allocation converges to Nash equilibrium within 10 iterations.

Author Contributions: Conceptualization, L.J.; methodology, L.J.; software, L.J.; validation, P.L.; formal analysis, P.L.; investigation, Y.Y.; resources, Y.Y.; data curation, L.X.; writing—original draft preparation, L.X.; writing—review and editing, Q.C.; visualization, Q.C.; supervision, J.Y., X.Y. and X.X.; project administration, J.Y., X.Y. and X.X.; funding acquisition, J.Y., X.Y. and X.X. All authors have read and agreed to the published version of the manuscript.

Funding: This research was funded by the National Key Laboratory of Science and Technology on Radar Detection and Sensing, and the High-level Innovation and Entrepreneurship Talent Introduction Program Team of Jiangsu Province.

Institutional Review Board Statement: Not applicable.

Informed Consent Statement: Not applicable.

Data Availability Statement: The raw data supporting the conclusions of this article will be made available by the authors on request.

Acknowledgments: During the writing phase of this manuscript, the authors used Google Gemini 3.1 Pro only for language editing. All outputs were reviewed and revised by the authors, who take full responsibility for the final content.

Conflicts of Interest: The authors declare no conflicts of interest.

Abbreviations

The following abbreviations are used in this manuscript:

UL/DL	Uplink/Downlink
SBS	Small Base Station
MBS	Macro Base Station
C-V2X	Cellular Vehicle-to-Everything
B5G	Beyond 5G
6G	Sixth Generation
WSP	Wireless Service Provider
ITS	Intelligent Transportation System
SINR	Signal-to-Interference-plus-Noise-Ratio
PPP	Poisson Point Process
PLP	Poisson Line Process
PDF	Probability Density Function
CDF	Cumulative Distribution Function
PGFL	Probability Generating Functional

References

1. Bazzi, A.; Ying, M.; Kanhere, O.; Rappaport, T.S.; Chafii, M. ISAC imaging by channel state information using ray tracing for next generation 6G. *IEEE J. Sel. Top. Electromagn. Antennas Propag.* **2025**, *1*, 135–149. [CrossRef]
2. Xiong, J.; Guo, H.; Liu, J. Intelligent task offloading for heterogeneous V2X communications. *IEEE Trans. Intell. Transp. Syst.* **2020**, *22*, 2226–2238. [CrossRef]
3. Qian, B.; Zhou, H.; Ma, T.; Xu, Y.; Yu, K.; Shen, X.S.; Hou, F. Leveraging dynamic Stackelberg pricing game for multi-mode spectrum sharing in 5G-VANET. *IEEE Trans. Veh. Technol.* **2020**, *69*, 6374–6387. [CrossRef]
4. Ali, M.A.; Khan, S.A.; Aldirmaz Colak, S.; Kosunalp, S.; Iliev, T. Towards 6G C-V2X Networks: A Comprehensive Survey on Mobility Management, Multi-RAT Coexistence, and Machine Learning (3M) Framework for C-ITS. *Electronics* **2026**, *15*, 1042. [CrossRef]
5. Andrews, J.G.; Baccelli, F.; Ganti, R.K. A tractable approach to coverage and rate in cellular networks. *IEEE Trans. Commun.* **2011**, *59*, 3122–3134. [CrossRef]
6. Ghosh, A.; Mangalvedhe, N.; Ratasuk, R.; Mondal, B.; Cudak, M.; Visotsky, E.; Thomas, T.A.; Andrews, J.G.; Xia, P.; Jo, H.S.; et al. Heterogeneous cellular networks: From theory to practice. *IEEE Commun. Mag.* **2012**, *50*, 54–64. [CrossRef]
7. Yin, X.; Liu, J.; Cheng, X.; Xiong, X. A C-V2X compatible massive data download scheme based on heterogeneous vehicular network. *IEEE Trans. Consum. Electron.* **2023**, *69*, 962–973. [CrossRef]
8. Xu, Y.; Qian, B.; Yu, K.; Ma, T.; Zhao, L.; Zhou, H. Federated Learning Over Fully-Decoupled RAN Architecture for Two-Tier Computing Acceleration. *IEEE J. Sel. Areas Commun.* **2023**, *41*, 789–801. [CrossRef]
9. Jiao, L.; Yu, K.; Xu, Y.; Zhang, T.; Zhou, H.; Shen, X. Spectral Efficiency Analysis of Uplink-Downlink Decoupled Access in C-V2X Networks. In *GLOBECOM 2022—2022 IEEE Global Communications Conference*; IEEE: Piscataway, NJ, USA, 2022; pp. 2062–2067.
10. Elshaer, H.; Kulkarni, M.N.; Boccardi, F.; Andrews, J.G.; Dohler, M. Downlink and uplink cell association with traditional macrocells and millimeter wave small cells. *IEEE Trans. Wirel. Commun.* **2016**, *15*, 6244–6258. [CrossRef]
11. Wu, P.; Ding, L.; Wang, Y.; Li, L.; Zheng, H.; Zhang, J. Performance analysis for uplink transmission in user-centric ultra-dense V2I networks. *IEEE Trans. Veh. Technol.* **2020**, *69*, 9342–9355.
12. Boccardi, F.; Heath, R.W.; Lozano, A.; Marzetta, T.L.; Popovski, P. Five disruptive technology directions for 5G. *IEEE Commun. Mag.* **2014**, *52*, 74–80. [CrossRef]
13. Xu, Y.; Liu, Z.; Qian, B.; Du, H.; Chen, J.; Kang, J.; Zhou, H.; Niyato, D. Fully-Decoupled RAN for Feedback-Free Multi-Base Station Transmission in MIMO-OFDM System. *IEEE J. Sel. Areas Commun.* **2025**, *43*, 780–794. [CrossRef]
14. Shi, D.; Chen, T.; Shi, L. A survey on intelligent control for multiagent systems. *IEEE Trans. Syst. Man Cybern. Syst.* **2022**, *51*, 161–175. [CrossRef]
15. Jiao, L.; Yu, K.; Chen, J.; Liu, T.; Zhou, H.; Cai, L. Performance Analysis of Uplink/Downlink Decoupled Access in Cellular-V2X Networks. *IEEE Trans. Mob. Comput.* **2023**, *23*, 5616–5630. [CrossRef]
16. Chetlur, V.V.; Dhillon, H.S. Coverage analysis of a vehicular network modeled as Cox process driven by Poisson line process. *IEEE Trans. Wirel. Commun.* **2018**, *17*, 4401–4416. [CrossRef]
17. Xu, C.; Sheng, M.; Yang, C.; Wang, X.; Wang, L. Wireless service provider selection and bandwidth resource allocation in multi-tier HCNs. *IEEE Trans. Commun.* **2016**, *64*, 5108–5124. [CrossRef]
18. Ahsan Kazmi, S.M.; Tran, N.H.; Ho, T.M.; Hong, C.S. Hierarchical Matching Game for Service Selection and Resource Purchasing in Wireless Network Virtualization. *IEEE Commun. Lett.* **2017**, *22*, 121–124. [CrossRef]
19. Dhillon, H.S.; Ganti, R.K.; Baccelli, F.; Andrews, J.G. Modeling and analysis of K-tier downlink heterogeneous cellular networks. *IEEE J. Sel. Areas Commun.* **2012**, *30*, 550–560. [CrossRef]
20. Jo, H.S.; Sang, Y.J.; Xia, P.; Andrews, J.G. Heterogeneous cellular networks with flexible cell association: A comprehensive downlink SINR analysis. *IEEE Trans. Wirel. Commun.* **2012**, *11*, 3484–3495. [CrossRef]
21. Lu, X.; Salehi, M.; Haenggi, M.; Hossain, E.; Jiang, H. Stochastic geometry analysis of spatial-temporal performance in wireless networks: A tutorial. *IEEE Commun. Surv. Tutor.* **2021**, *23*, 2753–2801. [CrossRef]
22. Sattar, Z.; Evangelista, J.V.; Kaddoum, G.; Batani, N. Spectral efficiency analysis of the decoupled access for downlink and uplink in two-tier network. *IEEE Trans. Veh. Technol.* **2019**, *68*, 4871–4883. [CrossRef]
23. Wu, Y.; Zhu, Q.; Huang, J.; Tsang, D.H.K. Revenue sharing based resource allocation for dynamic spectrum access networks. *IEEE J. Sel. Areas Commun.* **2014**, *32*, 2280–2296. [CrossRef]
24. Niyato, D.; Hossain, E. Competitive pricing for spectrum sharing in cognitive radio networks: Dynamic game, inefficiency of Nash equilibrium, and collusion. *IEEE J. Sel. Areas Commun.* **2009**, *26*, 192–202. [CrossRef]
25. Liang, L.; Ye, H.; Li, G.Y. Spectrum sharing in vehicular networks based on multi-agent reinforcement learning. *IEEE J. Sel. Areas Commun.* **2019**, *37*, 2282–2292. [CrossRef]
26. Chetlur, V.V.; Dhillon, H.S. Coverage and rate analysis of downlink cellular vehicle-to-everything (C-V2X) communication. *IEEE Trans. Wirel. Commun.* **2019**, *19*, 1738–1753.

27. Sand, S.; Unterhuber, P.; Ahmed, D.B.; Müller, F.D.P.; Lehner, A.; Rashdan, I.; Schmidhammer, M.; Karásek, R.; Siebler, B.; Heirich, O.; et al. Radio interference measurements for urban cooperative intelligent transportation systems. In *2021 IEEE 94th Vehicular Technology Conference (VTC2021-Fall)*; IEEE: Piscataway, NJ, USA, 2021; pp. 1–6.
28. Stoica, P.; Moses, R.L. *Spectral Analysis of Signals*; Pearson Prentice Hall: Upper Saddle River, NJ, USA, 2005; Volume 452.
29. Chiu, S.N.; Stoyan, D.; Kendall, W.S.; Mecke, J. *Stochastic Geometry and Its Applications*; John Wiley & Sons: Hoboken, NJ, USA, 2013.
30. Chen, C. Approximation for probability of coverage in softly inhibitive cellular networks. *Electron. Lett.* **2024**, *60*, e70005. [CrossRef]
31. Ofcom. *Award of the 2.3 and 3.4 GHz Spectrum Bands*; Office of Communications: London, UK, 2018.
32. Sandholm, W.H. Evolutionary game theory. In *Complex Social and Behavioral Systems: Game Theory and Agent-Based Models*; Springer: New York, NY, USA, 2020; pp. 573–608.

Disclaimer/Publisher's Note: The statements, opinions and data contained in all publications are solely those of the individual author(s) and contributor(s) and not of MDPI and/or the editor(s). MDPI and/or the editor(s) disclaim responsibility for any injury to people or property resulting from any ideas, methods, instructions or products referred to in the content.